THE ASTROPHYSICAL JOURNAL, 495:157–169, 1998 March 1

GRAVITATIONAL LENSING BY SPIRAL GALAXIES

C. R. KEETON AND C. S. KOCHANEK
Harvard-Smithsonian Center for Astrophysics, MS-51, 60 Garden Street, Cambridge, MA 02138; ckeeton@cfa.harvard.edu, ckochanek@cfa.harvard.edu
Received 1997 June 5; accepted 1997 October 7

ABSTRACT

We study gravitational lensing by spiral galaxies, using realistic models consisting of halo, disk, and bulge components combined to produce a flat rotation curve. Proper dynamical normalization of the models is critical because a disk has less (projected) mass than does a spherical halo with the same rotation curve—a face-on Mestel disk has a lensing cross section only 41% as large as that of a comparable singular isothermal sphere. Lensing cross sections are sensitive to inclination and are dominated by edge-on galaxies that, if very flattened, produce a large number of lenses with an unobserved image geometry consisting of 2 or 3 images off to one side of the galaxy center and straddling the projected disk. The absence of this "disk" image geometry among known lenses suggests that lens galaxies cannot be highly flattened. When averaged over inclination, disk+halo models predict $\lesssim 10\%$ more lenses than do pure halo models, except in cases in which the disk is unreasonably massive, so including a disk does not significantly increase the expected number of spiral galaxy lenses. Models with an exponential disk and a central bulge are sensitive to the properties of the bulge. In particular, an exponential disk model normalized to our Galaxy but without a bulge cannot produce multiple images, and including a bulge reduces the net flattening of edge-on galaxies. The dependence of the lensing properties on the masses and shapes of the halo, disk, and bulge means that a sample of spiral galaxy lenses would provide useful constraints on galactic structure.

Subject headings: galaxies: spiral — galaxies: structure — gravitational lensing

1. INTRODUCTION

Simple theoretical models of spherical gravitational lenses predict that spiral galaxies produce only 10%–20% of gravitational lenses (Turner, Ostriker, & Gott 1984; Fukugita & Turner 1991; Maoz & Rix 1993; Kochanek 1991, 1993, 1996a). This prediction is roughly consistent with observations (see Keeton, Kochanek, & Falco 1997a). Specifically, of ~ 30 known lenses,[1] only B0218+357 (O'Dea et al. 1992; Patnaik et al. 1993) is produced by a galaxy unambiguously identified as a distant spiral galaxy based on its color and mass-to-light ratio, as well as on the presence of H I and molecular gas and strong Faraday rotation (Patnaik et al. 1993; Carilli, Rupen, & Yanny 1993; Wiklind & Combes 1995; Combes & Wiklind 1997; Keeton et al. 1997a). The lens B1600+434 (Jackson et al. 1995) has a galaxy identified as a spiral (Jaunsen & Hjorth 1997; Jackson, Nair, & Browne 1997), although with this interpretation its image separation and lens luminosity may be hard to reconcile (Keeton et al. 1997a). The lens Q2237+0305 (Huchra et al. 1985), found as part of a redshift survey, is a special case of lensing by the bulge of a nearby spiral galaxy ($z_l = 0.04$). The radio ring PKS 1830−211 (Rao & Subrahmanyan 1988; Jauncey et al. 1991) shows both H I and molecular absorption features (Lovell et al. 1996; Wiklind & Combes 1996) and thus may have a spiral lens galaxy, but because the absorption features are at different redshifts and because there is no optical identification of the lens galaxy, this lens is still not understood. The remaining lens galaxies are generally more consistent with early-type galaxies than with spirals (Keeton et al. 1997a).

Models of individual lenses and the observed numbers of four-image lenses seem to require mean axis ratios somewhat flatter than expected for early-type galaxies (Kochanek 1996b; King & Browne 1996; Keeton, Kochanek, & Seljak 1997b). The apparent discrepancy may be caused by difficulties in interpreting the axis ratios of lens models, a task complicated by the effects of external tidal shears from neighboring galaxies and clusters (see, e.g., Hogg & Blandford 1994; Schechter et al. 1997) and by the possibility that dark halos may be flatter than the light (see, e.g., Dubinski & Carlberg 1991; Sackett et al. 1994; Buote & Canizares 1994, 1996). An alternate possibility is that spherical models may grossly underestimate the number of spiral galaxy lenses by neglecting the effects of a flat disk. Any errors in estimating the expected number of lenses can bias inferences about the cosmological model based on the statistics of gravitational lenses, so there is growing interest in studying lensing by spirals using models that better represent real galaxies.

There are as yet no thorough treatments of lensing by spiral galaxies using a model that includes both a realistic disk and a halo. The original spherical models treated spiral galaxies as singular isothermal spheres (SIS) normalized by their rotation curves, so they represented diskless, pure halo models. Models using ellipsoidal densities (Kassiola & Kovner 1993; Kormann, Schneider, & Bartelmann 1994a, 1994b; Kochanek 1996b; Keeton et al. 1997b) can be interpreted as projections of disk galaxies without halos, although they are not generally viewed as such. Pure disk models are poor representations of spiral galaxies because they neglect the dynamically important dark halos that may not be spherical but are certainly not as flat as disks (see reviews by Ashman 1992; Rix 1996). In addition, a pure disk model with a flat rotation curve predicts that the cross section diverges as the disk becomes edge-on, and that the divergent cross section is dominated by image geometry consisting of two bright images offset from the center of the galaxy and straddling the projected disk. Among point-image lenses, we see only lenses consisting of two or four

[1] For a summary, see Keeton & Kochanek (1996).

images surrounding the center of the galaxy (for a summary, see Keeton & Kochanek 1996), so the absence of the "disk" image geometry gives direct evidence for rounder halos. What makes lensing by realistic spiral galaxies interesting, then, is not the effects of the thin disk, because the properties of pure disk models were already understood from studies of ellipsoidal lenses, but the effects of the halo in suppressing the divergent cross section and unphysical image geometry of a pure disk model.

The fact that the observational data are not consistent with pure disk models means that spiral gravitational lenses will provide a useful probe of the balance between the disk and the halo in spiral galaxies. In our own Galaxy, the constraint on the local surface mass density of the disk of $(75 \pm 25)\ M_\odot\ \mathrm{pc}^{-2}$ (Kuijken & Gilmore 1991; Bahcall, Flynn, & Gould 1992; also see Sackett 1997) is one of the weakest links in understanding the mass distribution of the Galaxy and in interpreting the results of LMC and Galactic bulge microlensing searches (see, e.g., Alcock et al. 1995). In external galaxies, the decomposition of rotation curves between the disk and the halo is usually degenerate and standard models assume a "maximal disk" to derive lower bounds on the halo contributions (see, e.g., van Albada & Sancisi 1986), although there has been some success in decomposing rotation curves (see, e.g., Persic, Salucci, & Stel 1996, and references therein). Thus any new constraint on the relative contributions of the disk and the halo in spiral galaxies has significance well beyond its particular effects on gravitational lensing.

Recently Maller, Flores, & Primack (1997) and Wang & Turner (1997) began to explore the effects of combining a disk with a halo. Maller et al. (1997) examined the ability of models with a halo and a constant density or an exponential disk to fit the lens B1600+434 and briefly considered broader lensing implications of their models. Wang & Turner (1997) used a constant surface-density disk to examine the inclination-averaged cross section and to see if the spherical models systematically underestimate the number of lenses produced by spirals. The constant-density disk model is analytically tractable, but its mass density and rotation curve bear little resemblance to those of a real galaxy, and the sharp disk edge introduces peculiar features in the lensing properties. Here we introduce several simple, physically reasonable models for lensing by spiral galaxies by combining halo, disk, and bulge components to produce nearly flat rotation curves. In § 2 we describe the halo, disk, and bulge components and discuss their lensing properties. In §§ 3 and 4 we combine the components into realistic models and study the effects of inclination and the shapes and masses of the halo, disk, and bulge on the lensing cross section, optical depth, and image geometries. In § 5 we summarize our results and discuss their implications for lensing statistics, galactic structure, and the statistics of damped Lyα absorbers.

2. MODEL COMPONENTS: DISKS, HALOS, AND BULGES

We build realistic models for spiral galaxies by embedding a thin disk and possibly a central bulge in a dark matter halo. We can describe both disky and spheroidal components by using an oblate spheroid with axis ratio q_3 and then letting $q_3 \to 0$ for an infinitely thin disk or $q_3 \lesssim 1$ for a moderately flattened halo or bulge. An oblate spheroid projects to an ellipsoidal density distribution with projected axis ratio $q = (q_3^2 \cos^2 i + \sin^2 i)^{1/2}$, where i is the inclination angle (such that $i = 90°$ is face-on and $i = 0°$ is edge-on). In the limit of an infinitely thin disk, a surface mass distribution $\Sigma_3(R^2)\delta(z)$ projects to an ellipsoid with surface density

$$\Sigma = \frac{1}{q}\,\Sigma_3\left(x^2 + \frac{y^2}{q^2}\right), \tag{1}$$

where $q = |\sin i|$. Thus the ellipsoidal gravitational lens models used by Kassiola & Kovner (1993), Kormann et al. (1994a, 1994b), Kochanek (1996b), and Keeton et al. (1997b) can be viewed in the traditional way as models of early-type galaxies (projections of three-dimensional ellipsoids) or can be reinterpreted as pure disk models of spiral galaxies (projections of a two-dimensional disk). However, the dynamical normalization differs for the two interpretations; we focus on the disk interpretation and occasionally discuss its relation to the early-type galaxy interpretation.

A simple building block for galaxies with flat rotation curves is the softened, oblate, "isothermal" density distribution. The density and rotation curve for this model are

$$\rho = \frac{v_c^2}{4\pi G q_3}\,\frac{e}{\sin^{-1} e}\,\frac{1}{s^2 + R^2 + z^2/q_3^2} \tag{2}$$

and

$$v_c^2(R) = v_c^2\left\{1 - \frac{e}{\sin^{-1} e}\,\frac{s}{(R^2 + e^2 s^2)^{1/2}} \times \tan^{-1}\left[\frac{(R^2 + e^2 s^2)^{1/2}}{q_3\, s}\right]\right\}, \tag{3}$$

where s is a core radius, $e = (1 - q_3^2)^{1/2}$ is the eccentricity of the mass distribution, and the model is normalized so that, asymptotically, $v_c(R) \to v_c$. The SIS model corresponds to the limit $q_3 = 1$ and $s = 0$. The projected surface mass density in units of the critical surface mass density for lensing is

$$2\Sigma/\Sigma_{\mathrm{cr}} = b_I[q^2(s^2 + x^2) + y^2]^{-1/2}, \tag{4}$$

where $b_I = b_{\mathrm{SIS}}\, e/\sin^{-1} e$, $b_{\mathrm{SIS}} = 2\pi(v_c/c)^2 D_{LS}/D_{OS}$ is the critical radius of a singular isothermal sphere with rotation velocity v_c, and D_{OS} and D_{LS} are comoving distances from the observer to the source and from the lens to the source, respectively. The lensing potential, deflection, and magnification produced by the lens are

$$\phi_I(s, q_3) = x\alpha_{,x} + y\alpha_{,y} - b_I\, s \ln[(\psi + s)^2 + (1 - q^2)x^2]^{1/2} + \text{constant}, \tag{5}$$

$$\alpha_{,x} = \frac{b_I}{(1 - q^2)^{1/2}}\,\tan^{-1}\left[\frac{(1 - q^2)^{1/2} x}{\psi + s}\right], \tag{6}$$

$$\alpha_{,y} = \frac{b_I}{(1 - q^2)^{1/2}}\,\tanh^{-1}\left[\frac{(1 - q^2)^{1/2} y}{\psi + q^2 s}\right], \tag{7}$$

and

$$M^{-1} = 1 - \frac{b_I}{\psi} + \frac{b_I^2\, s}{\psi[(\psi + s)^2 + (1 - q^2)x^2]}, \tag{8}$$

where $\psi^2 = q^2(s^2 + x^2) + y^2$. These equations are identical (up to an overall normalization factor) to those derived in previous treatments of the softened isothermal ellipsoid (see,

e.g., Kassiola & Kovner 1993; Kormann et al. 1994a), but the analytic forms are simpler. The normalization is such that a softened isothermal ellipsoid usually written as $2\Sigma/\Sigma_{cr} = b_{IE}[s_{IE}^2 + r^2(1 - \epsilon \cos 2\theta)]^{-1/2}$ can be written in the form above by identifying $b_I^2 = b_{IE}^2(1 + q^2)/2$, $s^2 = s_{IE}^2(1 + q^2)/2q^2$, and $q^2 = (1 - \epsilon)/(1 + \epsilon)$.

In the limit of an infinitely thin disk ($q_3 \to 0$), the "isothermal" model becomes a disk with the surface density and rotation curve pair

$$\Sigma_M(R, s) = \frac{v_c^2}{2\pi G} \frac{1}{(R^2 + s^2)^{1/2}},$$

$$v_c^2(R, s) = v_c^2\left[1 - \frac{s}{(R^2 + s^2)^{1/2}}\right] \quad (9)$$

(see Evans & Collett 1993). We call this model a softened Mestel disk, because, in the limit $s \to 0$, it becomes a Mestel (1963) disk, the surface density distribution producing a flat rotation curve. The lensing potential of the softened Mestel disk is $\phi_M(s) = \phi_I(s, q_3 \equiv 0)$, and the deflection scale $b_M = 2b_{SIS}/\pi$ is the limit of b_I as $e \to 1$. Note that although the mass inside a sphere of radius r is the same for the Mestel disk and the SIS, the mass inside a *cylinder* is not the same—and it is the mass inside a cylinder that is important for lensing. Because the Mestel disk has a smaller projected mass than an SIS with the same rotation velocity, one immediate consequence is that a face-on Mestel disk has an image separation smaller by $b_M/b_{SIS} = 2/\pi = 0.64$ and a lensing cross section smaller by $b_M^2/b_{SIS}^2 = 4/\pi^2 = 0.41$. As the inclination increases, the lensing cross section grows and in fact diverges when the Mestel disk becomes edge-on. We will study this divergence in § 3.2; the main result is that the cross section diverges not because the model neglects the finite thickness of the disk, but rather because the total mass of the disk diverges. One way to avoid the divergence is to smoothly truncate the Mestel disk by using the difference of two Mestel disk models, $\phi_T(s, a) = \phi_M(s) - \phi_M(a)$, where the truncation radius a is larger than the core radius s. The surface density of the truncated Mestel disk model is constant for $R < s$ (rising rotation curve), declines as $1/R$ for $s < R < a$ (flat rotation curve), and declines as $1/R^3$ for $R > a$ (Keplerian rotation curve). The truncated Mestel disk has a finite mass of $M = (a - s)v_c^2/G$. Note that if the truncated model is round rather than flat, its density $\rho \propto 1/[(r^2 + s^2)(r^2 + a^2)]$ is similar to that of a Jaffe (1983) model, $\rho \propto 1/[r^2(r + a)^2]$.

A second useful building block is an unnamed density distribution with $\rho \sim r^{-4}$, asymptotically. In terms of the total mass M, the density and rotation curve are

$$\rho = \frac{Ms}{\pi^2 q_3} \frac{1}{(s^2 + R^2 + z^2/q_3^2)^2} \quad (10)$$

and

$$v_c^2(R) = \frac{2GM}{\pi R}\left\{\frac{R^3}{(R^2 + e^2 s^2)^{3/2}} \tan^{-1}\left[\frac{(R^2 + e^2 s^2)^{1/2}}{q_3 s}\right] - \frac{q_3 s R^3}{(R^2 + s^2)(R^2 + e^2 s^2)}\right\}. \quad (11)$$

In projection, the surface mass density, lensing potential, deflection, and magnification are

$$2\Sigma/\Sigma_{cr} = b_K^2 q^2 s[q^2(s^2 + x^2) + y^2]^{-3/2}, \quad (12)$$

$$\phi_K(s, q_3) = b_K^2 \ln[(\psi + s)^2 + (1 - q^2)x^2]^{1/2} + \text{constant}, \quad (13)$$

$$\alpha_{,x} = \frac{b_K^2 x}{\psi} \frac{\psi + q^2 s}{(\psi + s)^2 + (1 - q^2)x^2}, \quad (14)$$

$$\alpha_{,y} = \frac{b_K^2 y}{\psi} \frac{\psi + s}{(\psi + s)^2 + (1 - q^2)x^2}, \quad (15)$$

and

$$M^{-1} = 1 - \frac{b_K^2 q^2 s}{\psi^3} - \frac{b_K^4 q^2 s}{\psi^3[(\psi + s)^2 + (1 - q^2)x^2]} - \frac{b_K^4[\psi^2(\psi + s)^2 - s(2\psi + s)(\psi + q^2 s)^2]}{\psi^4[(\psi + s)^2 + (1 - q^2)x^2]^2}, \quad (16)$$

where the deflection scale b_K is related to the mass by $M = \pi b_K^2 \Sigma_{cr}$. In the limit of an infinitely thin disk ($q_3 \to 0$), the model corresponds to a Kuzmin (1956) or Toomre (1962) Model I disk and can be used to approximate an exponential disk. It has the same mass and central surface density as an exponential disk of the form $\Sigma(R) = \Sigma_0 e^{-R/s}$, and the rotation curves differ by at most 16%. A true exponential disk in projection requires numerical integrals, making it cumbersome to use.

In §§ 3–4 below, we combine these disk, halo, and bulge components to produce reasonable representations of spiral galaxies. For each model, we use the net deflection and magnification to find the critical curves and caustics. We then integrate the caustics in the source plane to compute the lensing cross sections, using the topology of the caustics to identify the different image geometries (see Schneider, Ehlers, & Falco 1992). Finally, we integrate over redshift to obtain lensing optical depths. Where a cosmological model is required, we adopt $\Omega_0 = 1$ and $H_0 = 50$ km s^{-1} Mpc^{-1}.

3. TRUNCATED MESTEL DISKS IN SOFTENED ISOTHERMAL HALOS

We first consider models consisting of a truncated Mestel disk embedded in an oblate isothermal halo. A Mestel disk has a surface mass density that falls off as R^{-1} while observed spiral galaxies have luminosity densities that fall off as e^{-R/R_d}, so a Mestel disk cannot represent a galaxy with a constant mass-to-light ratio in the disk. Nevertheless, the Mestel disk is interesting to study because it is the simplest disk system with a flat rotation curve.

3.1. *Normalization of the Model*

For simplicity, we let the disk be singular ($s = 0$), so its only scale length is the truncation radius a_d. We place the disk in a softened isothermal halo and tune the ratio of the halo scale radius a_h to the disk truncation radius a_d to produce a flat rotation curve; Table 1 gives typical values of the ratio for a rotation curve that is flat to better than 2%. The inner rotation curve ($R < a_d$) is supported entirely by the disk, so this is a "maximal disk" model for a spiral galaxy (see, e.g., van Albada & Sancisi 1986). It is not known whether most spiral galaxies have maximal disks, although it is generally believed that our Galaxy has a disk that is only $\sim$50% of maximal (Bahcall 1984; Kuijken & Gilmore 1989, 1991; van der Kruit 1989; Kuijken 1995; but

TABLE 1

SCALE LENGTH RATIO a_h/a_d FOR A FLAT ROTATION CURVE

	q_{3d}			
q_{3h}	0.1	0.03	0.01	0.0
$\frac{1}{3}$.....	0.9091	0.8801	0.8717	0.8675
$\frac{1}{2}$.....	0.8569	0.8296	0.8217	0.8177
1.....	0.7397	0.7161	0.7092	0.7058

NOTE.—Values of the ratio a_h/a_d needed to produce a flat rotation curve in a model with a truncated Mestel disk in a softened isothermal halo, where q_{3d} and q_{3h} are the axis ratios of the disk and halo, respectively. These values give a rotation curve that is flat to better than 2%.

see Sackett 1997 for a recent rebuttal). We allow for a submaximal disk, i.e., for some of the inner rotation curve to be supported by a dark matter halo, by embedding the disk + softened halo system in a singular isothermal halo. The overall lensing model is then

$$\phi = f_d[\phi_I(0, q_{3d}) - \phi_I(a_d, q_{3d}) + \phi_I(a_h, q_{3h})] + (1 - f_d)\phi_I(0, q_{3h}) , \quad (17)$$

where the "disk fraction" f_d is the fraction of the inner rotation curve supplied by the disk, and q_{3d} and q_{3h} are the three-dimensional axis ratios of the disk and halo, respectively. An infinitely thin disk has $q_{3d} = 0$ and a spherical halo has $q_{3h} = 1$. The projected axis ratios of the disk and halo are $q_d = (q_{3d}^2 \cos^2 i + \sin^2 i)^{1/2}$ and $q_h = (q_{3h}^2 \cos^2 i + \sin^2 i)^{1/2}$. The model contains the limits of a pure Mestel disk ($f_d = 1$ and $a_d \to \infty$) and a pure isothermal halo (either $f_d = 0$ or $a_d \to 0$). It has no bulge component and a singular central surface density.

Given a rotation velocity v_c, it is convenient to normalize the length scales by the critical radius $b_{\rm SIS}$ of the SIS model with the same circular velocity, which yields lensing cross sections in units of the SIS cross section ($\sigma_{\rm SIS} = \pi b_{\rm SIS}^2$) and thus indicates whether including the disk increases or decreases the cross section. We choose values for the disk and halo axis ratios q_{3d} and q_{3h}, the disk truncation radius a_d, and the disk fraction f_d and finally determine the halo core radius a_h from the value of a_h/a_d that gives a flat rotation curve (see Table 1).

For the physical normalization, we can compare the model with the Galaxy; we use the IAU value for the circular velocity $\Theta_0 = 220$ km s^{-1} (Kerr & Lynden-Bell 1986) and a consensus value for the solar radius $R_0 = 8$ kpc that is slightly smaller than the IAU value of 8.5 kpc (see the review by Reid 1993). The surface mass density of the disk at R_0 is

$$\Sigma_\odot = 350 f_d \frac{e_d}{\sin^{-1} e_d} \left(\frac{\Theta_0}{220 \text{ km s}^{-1}}\right)^2 \left(\frac{8 \text{ kpc}}{R_0}\right) \times \left[1 - \frac{R_0}{(R_0^2 + a_d^2)^{1/2}}\right] M_\odot \text{ pc}^{-2} , \quad (18)$$

where $e_d = (1 - q_{3d}^2)^{1/2}$ is the eccentricity of the disk. Local estimates of the surface mass density of the disk are 75 ± 25 $M_\odot$ pc^{-2}, with more of a consensus toward low values (Kuijken & Gilmore 1991; Bahcall et al. 1992; also see Sackett 1997), so we must choose $a_d/R_0 \gtrsim 0.5$, and we should reduce the disk fraction f_d if $a_d/R_0 \gtrsim 2$. The physical scale a_d/R_0 is related to the dimensionless ratio $a_d/b_{\rm SIS}$ appearing in the lens models by

$$\frac{a_d}{b_{\rm SIS}} = 0.20 \frac{a_d}{R_0} \left(\frac{R_0}{8\ h_{50}^{-1} \text{ kpc}}\right)\left(\frac{220 \text{ km s}^{-1}}{\Theta_0}\right)^2 \times \frac{2 r_H (1 + z_l) D_{OS}}{D_{OL} D_{LS}} , \quad (19)$$

where $r_H = c/H_0$ is the Hubble radius, D_{OL}, D_{OS}, and D_{LS} are comoving distances to the lens, to the source, and from the lens to the source, respectively, {with $D_{ij} = 2r_H[(1 + z_i)^{-1} - (1 + z_j)^{-1}]$ for $\Omega_0 = 1$}, and $H_0 = 50\ h_{50}$ km s^{-1} Mpc^{-1}. With $f_d = 1$, the disk dominates the inner rotation curve of the model provided $a_d/b_{\rm SIS} \gg 1$, which is always true because the minimum value of the cosmological distance ratio is ~ 10.

3.2. *The Effects of Inclination*

We first consider maximal disk models ($f_d = 1$), so the inner rotation curve is supported entirely by the disk. The lensing properties of the model depend strongly on both the inclination (through the axis ratio q_d) and the size (truncation radius a_d) of the disk. Figures 1 and 2 illustrate the critical curves, caustics, image geometries, and cross sections as functions of a_d and q_d.

For a face-on galaxy ($q_d = 1$), the model is strictly circular and the only multiple image geometry has three images (with one trapped and demagnified in the singular core of the disk). A nonaxisymmetric galaxy would also have a five-image cross section, but studies of face-on spiral galaxies indicate that they have axis ratios $b/a \gtrsim 0.7$ (see the review by Rix 1996) so the five-image cross section would be small. We noted in § 2 that a disk requires considerably less (projected) mass than does a spherical halo to produce a given rotation velocity, so the critical radius of a pure Mestel disk ($a_d \to \infty$) is smaller than that of the corresponding SIS by $b_{\rm M}/b_{\rm SIS} = 2/\pi$. Thus a face-on Mestel disk has a cross section $\sigma_{\rm M}/\sigma_{\rm SIS} = 4/\pi^2 = 0.41$, making it less efficient than an SIS at producing multiple images. As we truncate the Mestel disk, however, the isothermal halo supporting the outer rotation curve begins to increase the cross section, so $\sigma_I/\sigma_{\rm SIS}$ depends on the truncation radius a_d and varies from $4/\pi^2$ for $a_d \to \infty$ to unity for $a_d = 0$.

For a modestly inclined galaxy ($q_d \lesssim 1$), the tangential critical line becomes elongated and produces an "astroid" caustic corresponding to standard four-image geometries (see Schneider et al. 1992), with a fifth image trapped in the singular core of the disk. As the inclination increases (as q_d decreases), the tangential critical line becomes even more elongated and the astroid caustic pierces the radial caustic. The region inside the astroid caustic but outside the radial caustic corresponds to a configuration of three images on one side of the center of the galaxy. The middle image fades as the inclination increases (as q_d decreases), resulting in a geometry with two bright images off to one side of the galactic center and straddling the projected disk. This image geometry, which we refer to as the "disk" image geometry, has not been observed.

For a nearly edge-on galaxy ($q_d \ll 1$), the tangential critical line consists of a central round region with a narrow "spike" extending out along the x-axis, and the cross section diverges. There are two elements of the divergence. The first is the divergence of the radial caustic as $q_d \to 0$ and the surface mass density becomes a line density. For a disk

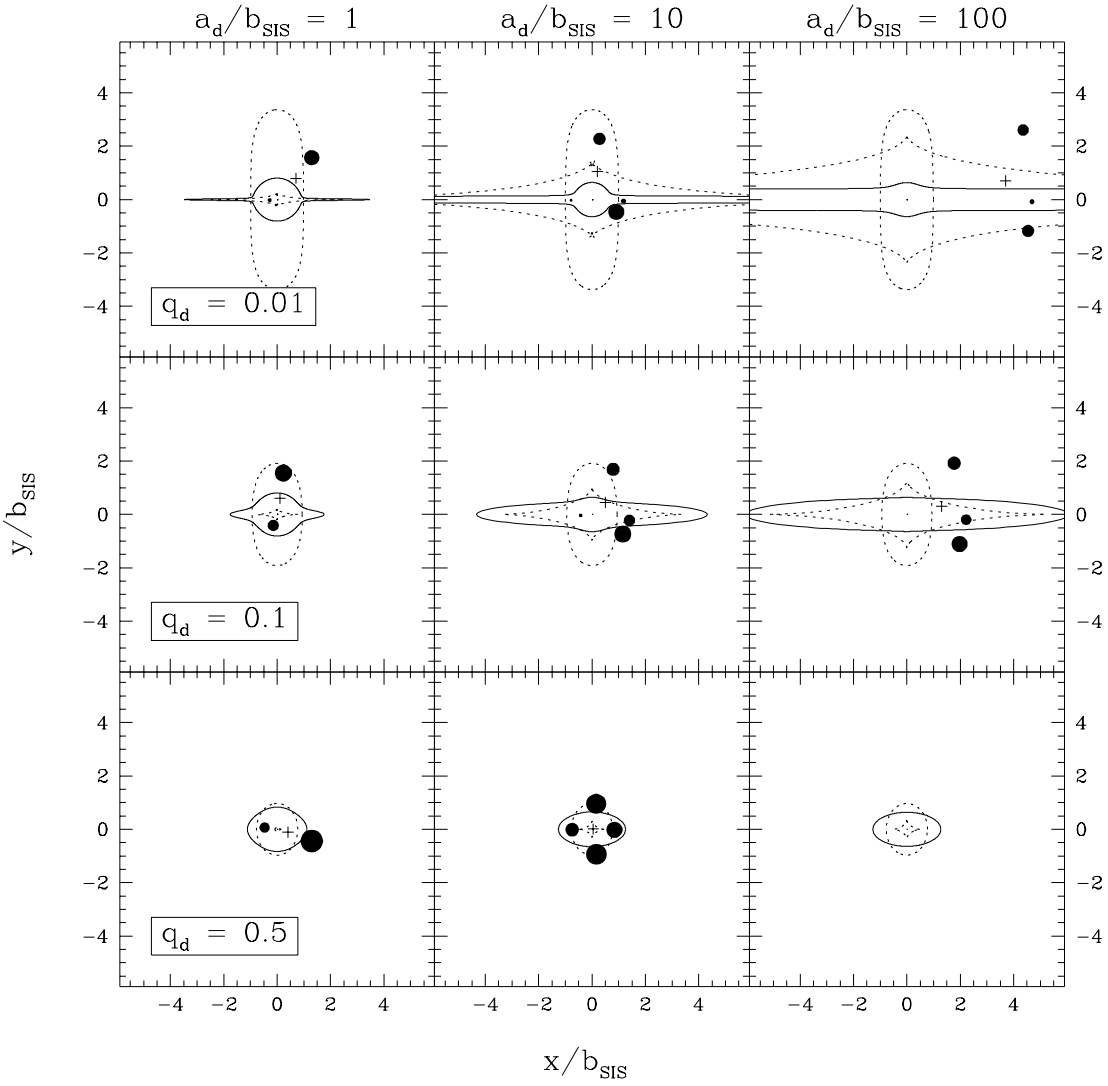

FIG. 1.—Sample critical curves, caustics, and image configurations for a truncated Mestel disk in a spherical isothermal halo. The projected disk axis ratio is $q_d = (q_{3d}^2 \cos^2 i + \sin^2 i)^{1/2}$. In each panel, the solid line is the tangential critical curve in the image plane, and the dotted lines are the tangential and radial caustics in the source plane. The three primary image geometries are illustrated with filled circles indicating images produced by a source marked with a plus. The standard two-image geometry is shown in the panels with $a_d/b_{SIS} = 1$, the four-image geometry in the panels with $a_d/b_{SIS} = 10$, and the unobserved "disk" geometry in the panels with $a_d/b_{SIS} = 100$. The two-image and four-image geometries each have an additional image trapped and demagnified in the singular core of the disk. The areas of the circles denote the magnifications.

with a core radius s that is small compared with the disk truncation radius a_d and with the halo scale radius a_h, the radial caustic is determined entirely by the central part of the disk and is independent of a_d and a_h. The radial caustic moves out along the y-axis as $|\ln q_d|$, and the three-image cross section diverges logarithmically. The divergence is unobservable because most of the large cross section corresponds to image geometries where the fluxes differ by orders of magnitude. This is analogous to the divergent cross section of a point-mass lens (see Schneider et al. 1992), which is formally infinite only because it allows images to pass arbitrarily close to a singular mass distribution and to be arbitrarily faint. In practice, spiral galaxy disks are observed to have a finite thickness; for example, Guthrie (1992) found a mean axis ratio of $q_{3d} = 0.11$ in a sample of edge-on spiral galaxies. A finite disk thickness prevents the mass density from becoming a singular line density and hence prevents the cross section from diverging.

The second element is the divergence of the astroid caustic as the mass of the disk diverges. In the limits of an edge-on galaxy ($q_d = 0$) or a pure Mestel disk ($a_d \to \infty$), the asymptotic cross sections are

$$\frac{\sigma_{\rm astr}}{\sigma_{\rm SIS}} \simeq \begin{cases} (4/\pi^2) q_d^{-1} & a_d/b_{\rm SIS} \gg q_d^{-1} \gg 1 , \\ (4/\pi) a_d/b_{\rm SIS} & q_d^{-1} \gg a_d/b_{\rm SIS} \gg 1 , \end{cases} \tag{20}$$

where $\sigma_{\rm astr} = \sigma_{\rm disk} + \sigma_5$ is the area of the astroid caustic. Results for intermediate regimes are shown in Figure 2. An edge-on disk ($q_d = 0$) has an astroid cross section $\sigma_{\rm astr} \propto a_d \propto M_d$, where M_d is the disk mass, so that the astroid cross section is finite provided M_d is finite. This means that the astroid cross section of a pure Mestel disk diverges because the mass diverges, not because the disk is infinitely thin. Although the cross section is finite for a truncated disk, it can still be quite large compared to that of an SIS model. Because most of the astroid lies outside the radial caustic, a nearly edge-on disk is dominated by the "disk" image geometry.

In order to produce a realistic disk model and to avoid the unphysical logarithmic divergence of the radial caustic,

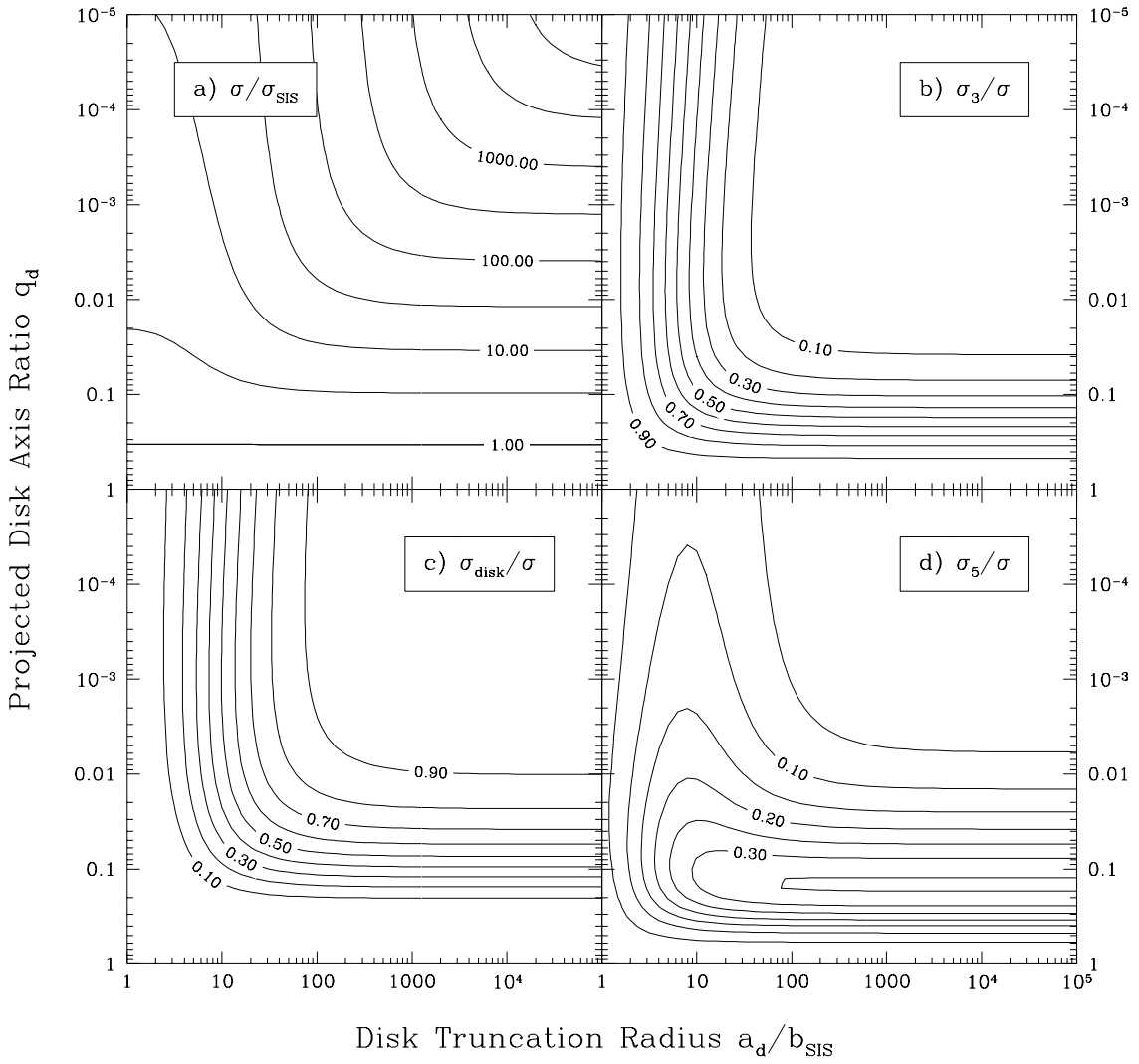

FIG. 2.—Cross sections for a truncated Mestel disk in a spherical isothermal halo as a function of the disk truncation radius a_d and the projected disk axis ratio $q_d = (q_{3d}^2 \cos^2 i + \sin^2 i)^{1/2}$. These are the cross sections for the critical curves and caustics depicted in Fig. 1. (*a*) Total cross section, with contours spaced logarithmically. (*b*)–(*d*) Branching ratios, or fractions of the total cross section, corresponding to three-image geometries, "disk" image geometries, and five-image geometries, respectively. In (*b*)–(*c*) the contour spacing is 0.1, and in (*d*) the contour spacing is 0.05.

we henceforth give the disk a finite thickness by making it an oblate spheroid with a small but nonzero q_{3d}. Spheroids are not ideal representations of the exponential vertical structure of disks, but because the details of the disk thickness matter only for inclinations with $\sin i \lesssim q_{3d}$, we use spheroids for analytic simplicity.

3.3. *The Effects of Disk and Halo Masses and Shapes*

We can characterize the expected contribution of spiral galaxies to lensing statistics by computing cross sections and optical depths averaged over inclination. In doing so, we neglect the magnification bias that, if included, would tend to reduce the inclination dependence of the five-image and disk geometry cross sections because the mean magnification is higher when the cross section is lower. Total probabilities, however, stay roughly proportional to the optical depth (see Wallington & Narayan 1993; Kochanek 1996b; Keeton et al. 1997b).

Figure 3 shows the inclination-averaged lensing cross section as a function of the disk truncation radius a_d/b_{SIS} and the disk fraction f_d for a disk with thickness $q_{3d} = 0.03$ in a spherical halo. Figure 4 shows the corresponding optical depth as a function of a_d/R_0. Note that a_d/R_0 is related to a_d/b_{SIS} by the redshift-dependent factor given in equation (19), so integrating over redshift to obtain the optical depth is equivalent to integrating over a_d/b_{SIS}. Somewhat surprisingly, although the face-on cross section is small and the edge-on cross section is large, the inclination-averaged cross section and optical depth (in units of the SIS values) are near unity. In other words, the disk + halo model does not significantly increase the number of lenses expected from spiral galaxies over the simple spherical SIS model. The number of lenses can be increased by $\sim 40\%$ only if a_d is large and f_d is near unity, corresponding to a disk that is much more massive than that in the Galaxy (Figs. 3*a* and 4*a*). Moreover, many of the additional lenses have the unobserved "disk" image geometry (Figs. 3*c* and 4*c*). Thus the disk + halo models that predict significantly more lenses than the spherical models are physically implausible, while models with a reasonable disk mass increase the total number of expected lenses by $\lesssim 10\%$.

Evidence from observations and from *N*-body simulations suggests that the dark halos of spirals are not spherical (see the reviews by Rix 1996 and Sackett 1996), so in

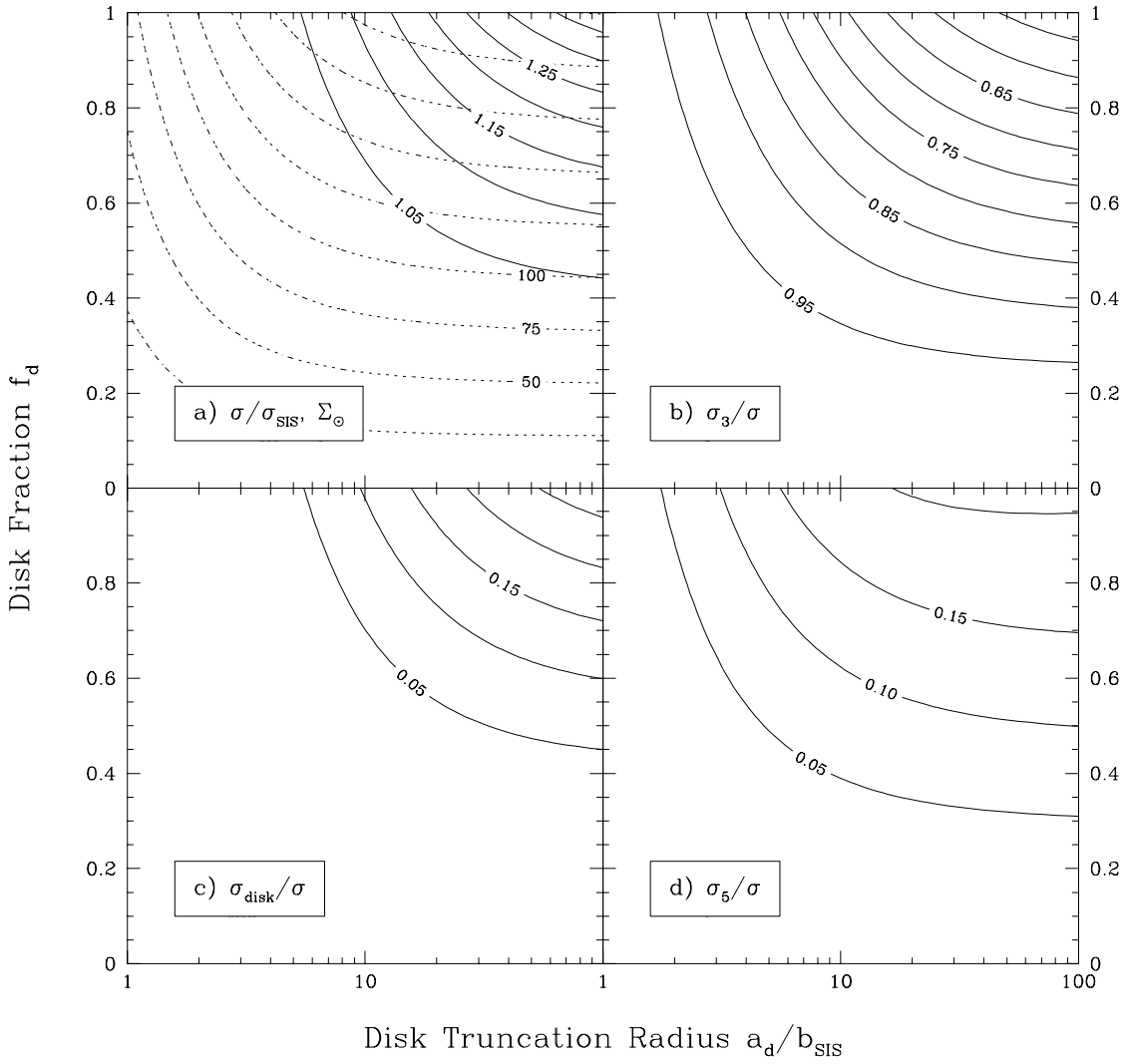

FIG. 3.—Inclination-averaged cross section and branching ratios for a truncated Mestel disk with a finite thickness $q_{3d} = 0.03$ in a spherical halo ($q_{3h} = 1$) as a function of the disk truncation radius a_d and the disk fraction f_d. The contour spacing is 0.05. Panel (*a*) also shows dotted lines indicating contours of the disk surface mass density at $R_0 = 8$ kpc for a circular velocity $\Theta_0 = 220$ km s^{-1} for a source at $z_s = 2$ and a lens galaxy at $z_l = 0.5$. The contour spacing is 25 $M_\odot$ pc^{-2}. The local estimate for the Galaxy is $\Sigma_\odot = (75 \pm 25)\, M_\odot$ pc^{-2}.

Figure 5 we consider the effects of flattening the halo. We also consider making the disk both thicker and thinner. Changing the disk thickness has little effect on the five-image lens fraction (τ_5/τ) but significantly changes the "disk" lens fraction (τ_{disk}/τ, not shown) and the total optical depth. This is because a thicker disk (larger q_{3d}) rules out the thin edge-on models that increase the cross section with numerous "disk" lenses. By contrast, making the halo oblate has little effect on the total optical depth but significantly changes the five-image and "disk" lens fractions. This makes sense because flattening the halo increases the net flattening of the system, thus causing more five-image and "disk" lenses while reducing the halo mass needed to produce the same rotation curve. The two effects conspire to keep the total optical depth essentially unchanged,[2] suggesting that flattening the halo—even to as flat as 3:1—does little to increase the total number of lenses. With any reasonably shaped halo, the only way to increase the number of lenses by $\sim 50\%$ compared to the simple SIS model is to let the mass of the system be dominated by the disk.

In addition to studying the expected number of lenses, we can also study their distribution with inclination. We use the optical depth distribution $d\tau_5/d(\sin i)$ to estimate the number of five-image lenses produced by a galaxy with inclination i. Although the distribution of spiral galaxies should be uniform in $\sin i$, we know from § 3.2 that the optical depth is dominated by nearly edge-on systems. The left-hand side of Figure 6 shows the median value of $\sin i$ for a model with $q_{3d} = 0.03$ and a 2:1 flattened halo. The results depend on q_{3d} and q_{3h}, but in most of the parameter space we have considered, the median value is less than $\sin 10° = 0.17$. In other words, because of the strong dependence of the cross section on the inclination, more than half of five-image lenses produced by spiral galaxies should come from systems with $|i| < 10°$, i.e., systems within 10° of being edge-on. The cross section for five-image lenses is strongly correlated with the cross section for

[2] For a singular isothermal ellipsoid normalized to a fixed equatorial rotation velocity, it can be shown analytically that the inclination average of $\sigma_3 + \sigma_5$ is independent of the axis ratio q_3 and exactly equal to the SIS cross section. As a result, the only increase in the lensing cross section is caused by "disk" images from flattened edge-on systems.

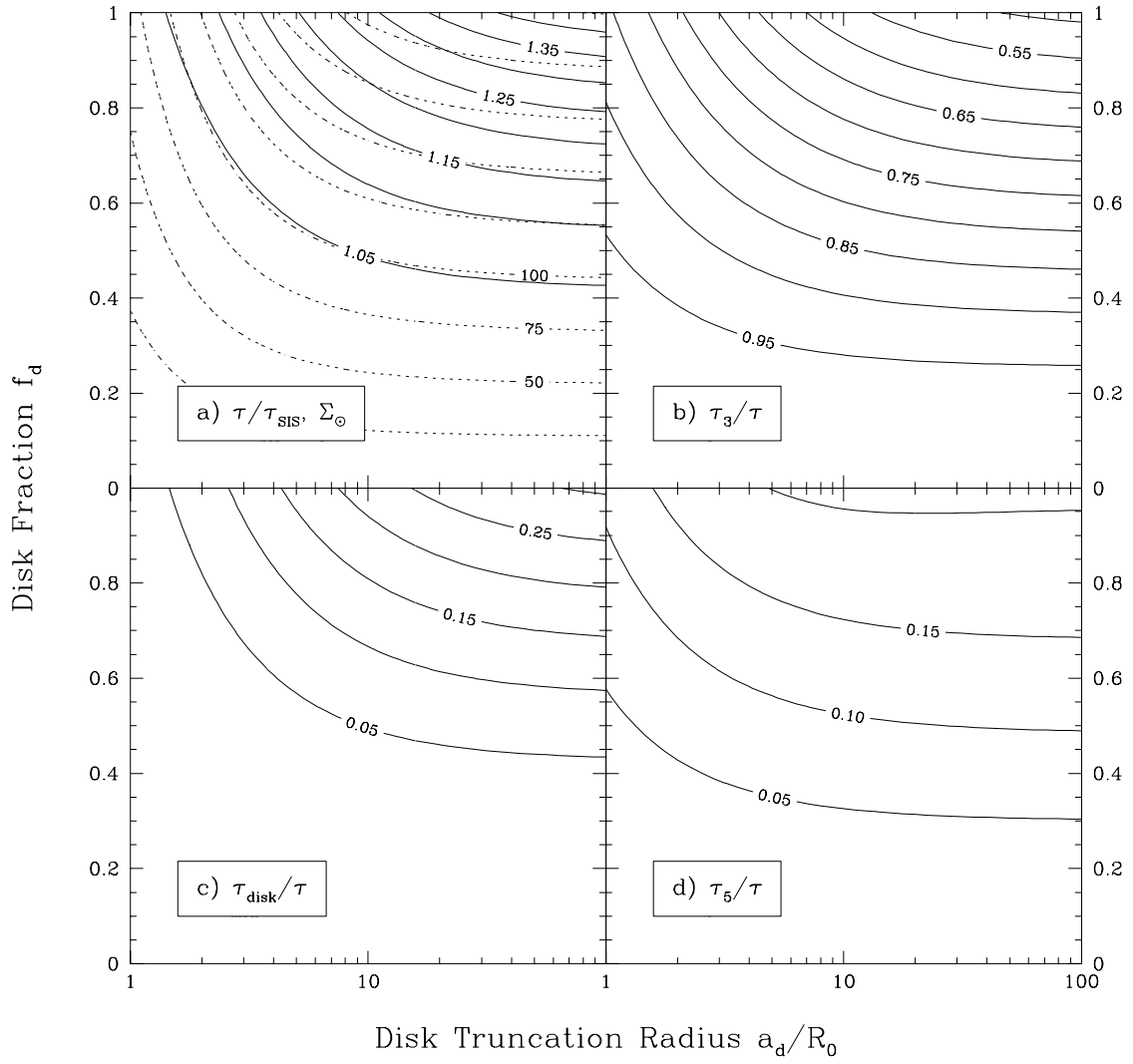

FIG. 4.—Inclination-averaged optical depth and branching ratios for the model in Fig. 3, where the optical depth is computed by integrating over lens redshift for a source at redshift $z_s = 2$. The contour spacing is 0.05. Panel (*a*) again shows dotted contours indicating the disk surface mass density at $R_0 = 8$ kpc for a circular velocity $\Theta_0 = 220$ km s^{-1}, with contours spaced every 25 $M_\odot$ pc^{-2}.

"disk" lenses because both image geometries are associated with the astroid caustic—the edge-on galaxies that produce most of the five-image lenses also produce "disk" lenses. However, the ratio of "disk" to five-image lenses does depend on the disk thickness. For example, a disk with thickness $q_{3d} = 0.03$ and a reasonable disk mass produces about half as many "disk" lenses as five-image lenses (see Figs. 4*c* and 4*d*), while a thicker disk eliminates thin edge-on models and hence reduces the number of "disk" lenses.

We noted in § 2 that disk lens models are closely related to ellipsoid lens models for early-type galaxies. One way to think about the relation is to compare the fractions of five-image lenses they produce. Figure 6*b* shows the axis ratio of the singular isothermal ellipsoid (SIE) that produces the same fraction of five-image lenses (i.e., the same τ_5/τ) as the inclination-averaged disk + halo model with $q_{3d} = 0.03$ and $q_{3h} = 0.5$. The results depend on q_{3d} and q_{3h}, but most models with a plausible disk mass have q_{SIE} between ~ 0.4 and ~ 0.6, with the flatter halos giving the lower values. In other words, in terms of the five-image lens fraction, inclination-averaged spiral galaxies correspond roughly to E4–E6 elliptical galaxies. One key difference, though, is that the elliptical galaxies would not produce lenses with the "disk" image geometry.

4. KUZMIN DISKS IN SOFTENED ISOTHERMAL HALOS

Real spiral galaxies have exponential disks and central bulges, so the inner regions are not well described by the Mestel disk models of § 3. We now use a Kuzmin disk as an approximation to an exponential disk, and we embed the disk in an isothermal halo to obtain the lensing model

$$\phi(\text{disk} + \text{halo}) = \phi_K(R_d, q_{3d}) + \phi_I(a_h, q_{3h}) , \qquad (21)$$

where R_d is the scale length of the exponential disk, and a_h is the scale radius of the halo. In § 3 we examined the effects of varying the disk thickness q_{3d} and the halo oblateness q_{3h}, so for simplicity we use a thin disk with $q_{3d} = 0.03$ and a 2:1 flattened halo ($q_{3h} = 0.5$). We have four remaining parameters (the scale lengths R_d and a_h, the disk mass M_d, and the asymptotic circular velocity v_c), but, by requiring that the disk + halo rotation curve be as flat as possible, we can fix two ratios,

$$GM_d/R_d v_c^2 = 2.577 \quad \text{and} \quad a_h/R_d = 2.229 . \qquad (22)$$

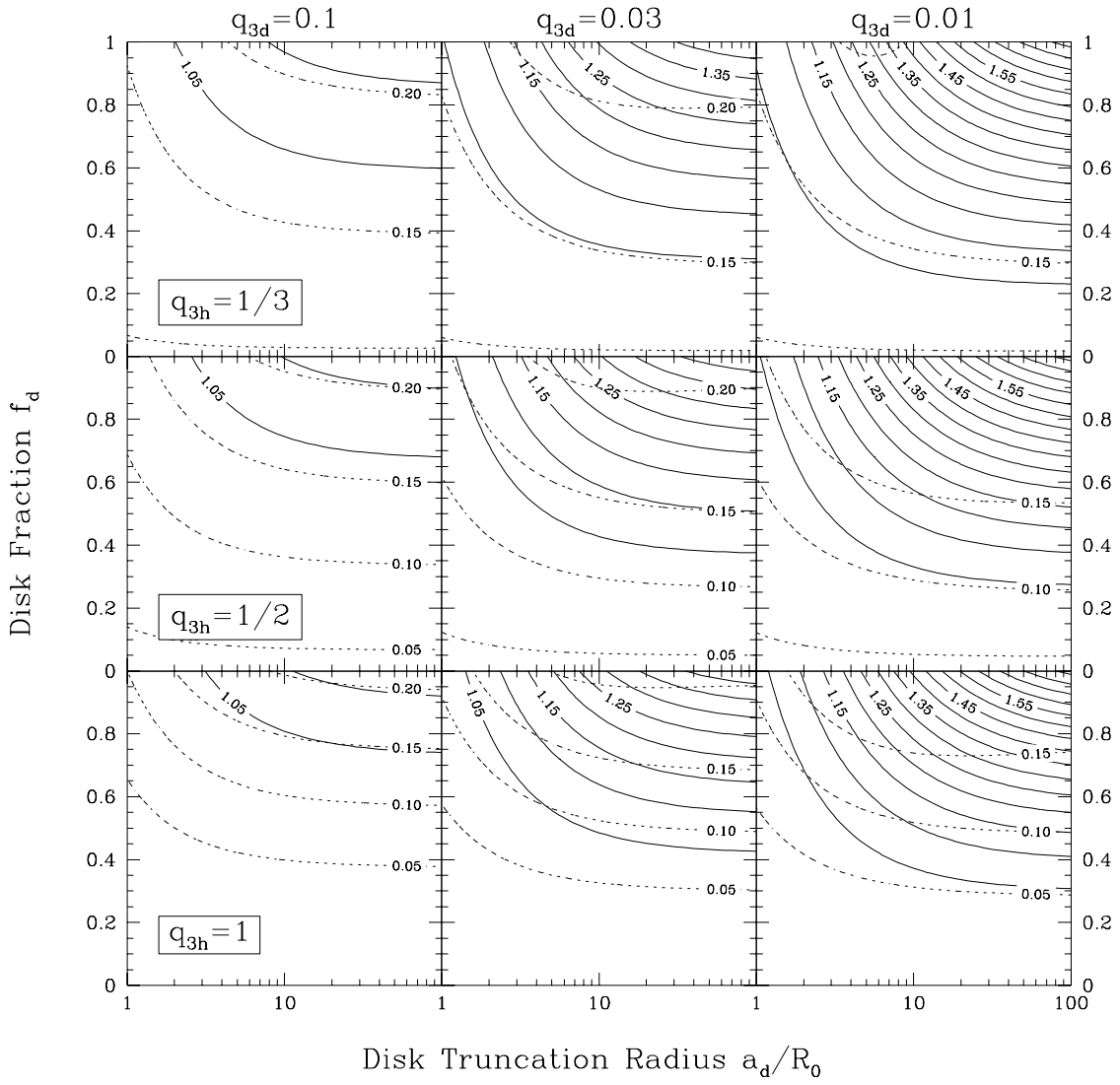

FIG. 5.—Contours of the inclination-averaged optical depth $\tau/\tau_{\rm SIS}$ (*solid lines*) and five-image lens fraction τ_5/τ (*dotted lines*) for a Mestel disk in an isothermal halo for various values of the disk thickness q_{3d} and halo oblateness q_{3h}. The contour spacing is 0.05. Moving up or to the right in the diagram increases the effective flattening of the galaxy.

With these constraints, the rotation curve starts at zero, rises to a peak 6% above v_c at $R = 1.8R_d$, falls to a minimum 0.6% below v_c at $R = 12.7R_d$, and then slowly asymptotes to v_c. We can then normalize the model, as in § 3, by using the Galaxy, which we take to have scale length $R_d = 3.5$kpc (see Sackett 1997). The local surface density and the total disk mass are then

$$\Sigma_\odot = 85\left(\frac{\Theta_0}{220\ \mathrm{km\ s^{-1}}}\right)^2\left(\frac{3.5\ \mathrm{kpc}}{R_d}\right) \times \left[\frac{1+(8/3.5)^2}{1+(R_0/R_d)^2}\right]^{3/2} M_\odot\ \mathrm{pc}^{-2} \qquad (23)$$

and

$$M_d = 10^{11}\left(\frac{\Theta_0}{220\ \mathrm{km\ s^{-1}}}\right)^2\left(\frac{R_d}{3.5\ \mathrm{kpc}}\right) M_\odot\ , \qquad (24)$$

so the disk is significantly more massive than the estimate of $6 \times 10^{10}\ M_\odot$ for our Galaxy (see, e.g., Bahcall 1986; Binney & Tremaine 1987), but the local surface mass density is consistent with the estimates of $75 \pm 25\ M_\odot\ \mathrm{pc}^{-2}$ (Kuijken & Gilmore 1991; Bahcall et al. 1992).

Combining the surface mass densities for the halo and disk from equations (4) and (12), the central surface mass density in units of the critical density for lensing is

$$\kappa_0 = \frac{1}{2}\left(\frac{b_h}{q_h a_h} + \frac{b_d^2}{q_d R_d^2}\right). \qquad (25)$$

A circular system is "supercritical," i.e., can produce multiple images, only if $\kappa_0 > 1$ (see Schneider et al. 1992). If we normalize the disk and halo as above and consider source and lens redshifts $z_s = 2$ and $z_l = 0.5$, then we have

$$a_h/b_{\rm SIS} = 2.784\ , \quad R_d/b_{\rm SIS} = 1.249\ , \quad \text{and} \quad b_d/b_{\rm SIS} = 1.431\ , \qquad (26)$$

so κ_0 does not exceed unity until $|\sin i| < 0.83$ or $|i| < 56°$. With a true exponential disk, the same analysis yields $a_h/b_{\rm SIS} = 2.747$ and $b_d/b_{\rm SIS} = 1.338$, so κ_0 does not exceed unity until $|i| < 48°$. Thus, nearly face-on systems (normalized to our Galaxy) are subcritical and cannot

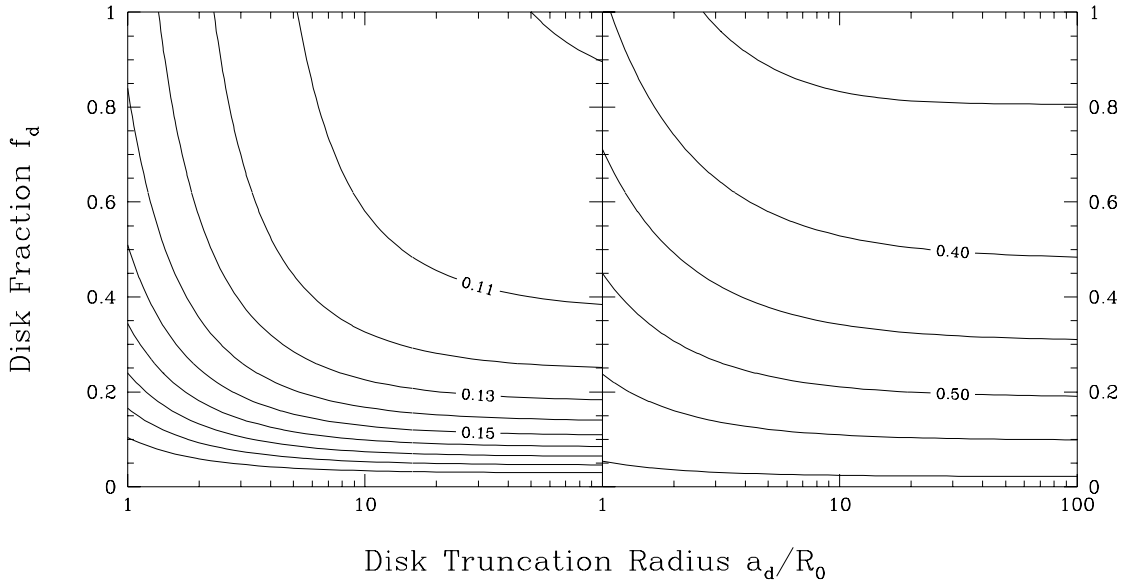

FIG. 6.—Properties of the distribution of five-image lenses for a truncated Mestel disk with thickness $q_{3d} = 0.03$ in a 2:1 flattened isothermal halo. *Left-hand panel*: Median value of sin i for the distribution of five-image lenses with inclination $[d\tau_5/d(\sin i)]$, with contour spacing 0.01. One-half of all five-image lens galaxies should be at least this close to edge-on. *Right-hand panel*: Axis ratio $q_{\rm SIE}$ of the singular isothermal ellipsoid producing the same fraction of five-image lenses (τ_5/τ) as the spiral galaxy model, with contour spacing 0.05.

produce multiple images. Modestly inclined systems are just barely supercritical, so although they can produce multiple images, their cross section for lensing is small.

Thus the low central surface density of the disk means that the bulge plays a crucial role in gravitational lensing by spiral galaxies. The bulge of our galaxy is well described by a de Vaucouleurs (1948) $r^{1/4}$ law (see, e.g., Bahcall 1986), but lensing by a de Vaucouleurs model is impractical because it requires five independent numerical integrals at every position. We could approximate the bulge with a modified Hubble profile, $\rho \propto [1 + (r/a)^2]^{-3/2}$, but the bulge mass $M_b(r)$ would diverge logarithmically, and we would be unable to characterize the bulge by its mass. So as a simple way to examine the qualitative effects of a central bulge with a finite mass, we use a bulge with the $\rho \sim r^{-4}$ profile discussed in § 2. The total lens model is then

$$\phi = \phi_{\rm K}(R_d, q_{3d}) + \phi_I(a_h, q_{3h}) + \phi_{\rm K}(a_b, q_{3b}) , \qquad (27)$$

where a_b is the scale radius and q_{3b} is the axis ratio for the bulge. For simplicity, we assume a fixed value for q_{3b}. A self-consistent disk + bulge model requires a flattened bulge (see, e.g., Monet, Richstone, & Schechter 1981), so, without attempting to build a self-consistent model, we fix $q_{3b} = 0.5$ for a 2:1 flattened bulge.

Figure 7 shows the inclination-averaged cross section for lensing as a function of the bulge mass M_b and the scale length a_b. The bulge strongly affects the cross section, primarily by controlling the central surface density. With a diffuse, low-mass bulge (large a_b and small M_b), the system is barely supercritical and the cross section is nonzero but small. As the bulge becomes massive and concentrated (a_b decreases and M_b increases), the cross section increases dramatically. The divergent cross section is misleading, though, because it is a point-mass divergence (see Schneider et al. 1992). Including magnification bias and limits on detectable flux ratios would reduce the cross section to a reasonable value. In addition to increasing the central surface density, the bulge also circularizes the center of the galaxy. As a result, the five-image and "disk" lenses that are associated with a flattened system become less significant as the bulge becomes more dominant (see Figs. 7*c* and 7*d*). Thus the bulge can regulate the number of five-image and "disk" lenses, and an analysis of the distribution of image geometries in a sample of spiral lenses must account for this effect.

Not all of the bulge parameter space in Figure 7 is physically reasonable. A concentrated bulge produces an unphysical mass distribution whose rotation curve has a strong central peak; in Figure 7*a* we show where the peak in the rotation curve caused by the bulge is 20% higher than the asymptotic circular velocity v_c. Conversely, a low-mass bulge cannot support the inner rotation curve; in Figure 7*a* we also show where the circular velocity at $R = R_d/2$ is only 80% of the asymptotic value. If we require that the inner rotation curve not deviate by more than 20% from v_c, then Figure 7 shows that the inclination-averaged cross section remains comparable to or smaller than the SIS result.

5. DISCUSSION

The traditional approach to gravitational lensing by spiral galaxies (Turner et al. 1984; Fukugita & Turner 1991; Maoz & Rix 1993; Kochanek 1991, 1993, 1996a) neglected the disk and used the dark halo alone to estimate that only 10%–20% of gravitational lenses should be produced by spiral galaxies. Recent ellipsoidal lens models (Kassiola & Kovner 1993; Kormann et al. 1994a, 1994b; Kochanek 1996b; Keeton et al. 1997b) can be reinterpreted as projections of disks to show that pure disk models viewed nearly edge-on can sharply increase the number of lenses compared with the pure halo models, but that most of the additional lenses have an unphysical "disk" image geometry with two bright images off to one side of the galactic center and straddling the projected disk. Thus it is important to have a halo to regulate the unphysical effects of a disk. Maller et al. (1997) recently considered constant-density and exponential disks in an isothermal halo in the context of modeling the lens B1600+434; Wang & Turner (1997)

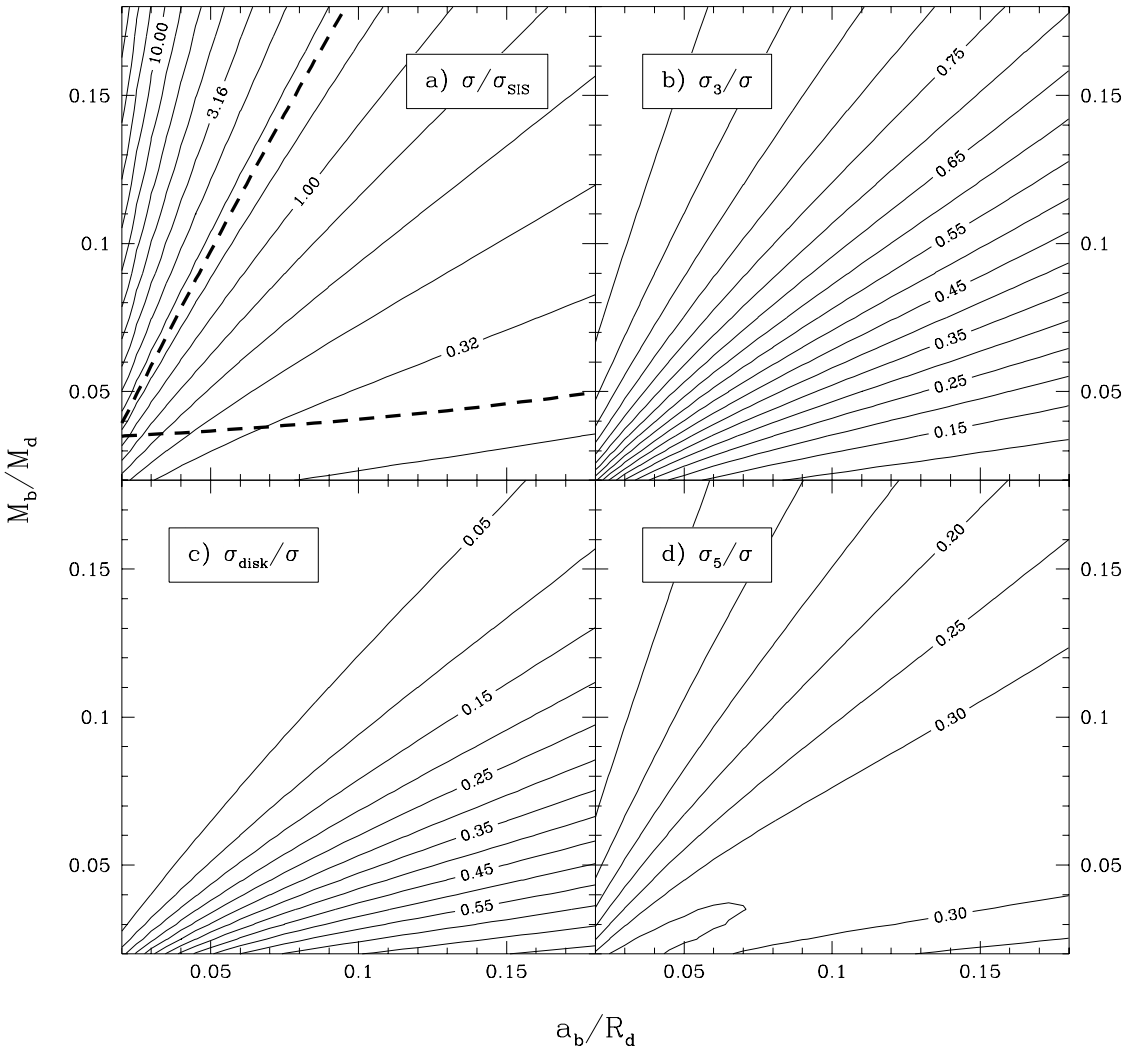

FIG. 7.—Inclination-averaged cross section and branching ratios for a Kuzmin disk in an isothermal halo as a function of the bulge-to-disk scale length ratio a_b/R_d and mass ratio M_b/M_d, where the disk and halo properties are held fixed. The halo and bulge are both 2:1 flattened. (*a*) Contours are spaced logarithmically. The heavy dashed lines indicate the range of parameters that give a reasonable rotation curve. Above the upper line, the bulge causes a central peak in the circular velocity that is at least 20% higher than the asymptotic velocity v_c. Below the lower line, the bulge cannot support the inner rotation curve and the velocity at one-half a disk scale length is at least 20% lower than the asymptotic velocity, i.e., $v_c(R_d/2) < 0.8v_c$. (*b*)–(*d*) Contour spacing is 0.05.

studied the general lensing properties of a constant density disk in an isothermal halo, but this model had a mass distribution and rotation curve very different from those of real galaxies. We have constructed physically plausible models by combining disk, halo, and bulge components normalized to produce a nearly flat rotation curve. We considered two classes of models: a truncated Mestel (1963) disk, which has dark matter in the disk, in an isothermal halo; and a Kuzmin (1956) disk as an approximation to an exponential disk, with a central bulge and an isothermal halo. These models reveal four distinctive features of lensing by spirals.

1. Proper dynamical normalization of the models is important. A disk requires less (projected) mass than does a spherical halo to produce the same rotation curve, so a disk model can have a lensing cross section significantly smaller than the corresponding halo model. For example, the cross section of a face-on Mestel disk is only 41% of the SIS cross section, and the cross section of a face-on exponential disk in an isothermal halo can be small or even zero (depending on the mass of the bulge).

2. The disk makes the lensing effects sensitive to the inclination. The cross section increases dramatically with inclination and is dominated by nearly edge-on models. For example, more than half of all five-image lenses produced by a Mestel disk galaxy come from galaxies within 10° of being edge-on. The cross section for five-image lenses is correlated with the cross section for lenses with the unobserved "disk" image geometry, so edge-on galaxies also produce significant numbers of "disk" lenses, although the disk thickness and a bulge offer ways to control the ratio of the two geometries.

3. Despite the inclination effects, disk + halo models averaged over inclination do not significantly increase the cross section (compared with pure halo models). The constant-density disk model of Wang & Turner (1997) predicted qualitatively that the disk can increase the cross section by at most $\sim 50\%$, and our models normalized to produce a given rotation curve restrict the increase to

$\lesssim 10\%$. Our models show that increasing the cross section or optical depth by even $\sim 50\%$ requires a very massive disk that dominates the dark halo, in conflict with observations that dark halos contribute significantly to spiral galaxy dynamics (see the review by Ashman 1992). Our conclusion is insensitive to the shape of the halo, even for a halo that is 3:1 flattened. Because of the dynamical normalization, flattening the halo changes the fraction of lenses with five-image or "disk" image geometries but has little effect on the total number of lenses.

4. A central bulge plays a crucial role in lensing by spiral galaxies with exponential disks because an exponential disk normalized to our Galaxy has a face-on central surface density too small to produce multiple images. The bulge raises the face-on central surface density enough to allow multiple imaging, with a diffuse bulge producing a small lensing cross section and a concentrated bulge producing a large cross section. The bulge also circularizes the center of the galaxy, diluting the effects of an edge-on disk and reducing the number of five-image and "disk" lenses. Replacing the bulge with a triaxial bar would give a face-on galaxy a small five-image cross section but would otherwise have little effect.

Our calculations neglected magnification bias so that we could perform large parameter surveys. Because mean magnifications tend to be large when cross sections are small, magnification bias would tend to reduce the inclination dependence of the five-image and "disk" image cross sections (see Schneider et al. 1992). In addition, magnification bias would increase the ratio of five-image and "disk" lenses (which have larger mean magnifications) to three-image lenses (which have smaller mean magnifications). Thus magnification bias is important for comparison to any observational sample. It should not, however, significantly affect the total cross section or the ratio of "disk" lenses to five-image lenses.

These results suggest that lensing by spiral galaxies can provide a new constraint on the structure of spiral galaxies. At present, the balance between disk and halo masses and the shapes of halos are poorly known. For example, the contribution of the Galactic disk to the rotation curve is not precisely known (Kuijken & Gilmore 1991; Bahcall et al. 1992; also see Sackett 1997), and it has been suggested that explaining the microlensing optical depth toward the Galactic bulge requires a disk that is heavier and closer to maximal than conventionally thought (see, e.g., Alcock et al. 1995). A sample of spiral galaxy lenses would constrain the relative masses and shapes of disks and halos, particularly if combined with *Hubble Space Telescope* images to determine the inclination of the disks. Discovering a lens with the "disk" image geometry would strongly constrain the disk surface mass density, while the continued absence of "disk" lenses would rule out disks with a surface density significantly higher than that of our Galaxy. Unfortunately, a large sample of spiral lenses may be difficult to obtain because they should contribute only 10%–20% of all lenses and because the small image separations and extinction in the lens galaxies may bias optical surveys against finding them.

Our results also have implications for the predicted correlation between gravitational lensing and damped Lyα absorption (also see Maller et al. 1997). Damped Lyα systems are thought to be associated with galactic disks (Wolfe 1988, 1995) and may thus produce lensing effects in background quasars. Bartelmann & Loeb (1996) and Smette, Claeskens, & Surdej (1997) have pointed out that lensing can affect the statistics of damped Lyα absorbers through magnification bias and by modifying the impact parameter. These analyses used the SIS lens model and thus neglected inclination effects in the lensing properties, although they did include inclination effects in the H I column density. The strong inclination dependence of the lensing properties must be taken into account in order to properly treat the effects of lensing on the statistics of damped Lyα absorbers.

Finally, our results suggest that spiral galaxies cannot easily explain the weak discrepancy between observed lens-galaxy axis ratios and the model axis ratios required to explain individual lenses and the statistics of four-image lenses (Kochanek 1996b; King & Browne 1996; Keeton et al. 1997b). While it is true that edge-on spiral galaxies can produce many four-image lenses, the absence of observed "disk" lenses indicates that spirals do not contribute significantly to the observational sample. Moreover, the disk does not substantially increase the total cross section compared with the SIS model. Thus the only way to increase the fraction of lenses caused by spirals is to change the ratio of spiral to early-type galaxy number densities. Kauffmann, Charlot, & White (1996) have offered evidence that evolution may reduce the number of early-type galaxies by as much as a factor of 2–3 at $z = 1$. However, most lens galaxies are closer than $z = 1$, and it seems unlikely that number evolution could change the ratio of spirals to early-type galaxies by the factor of ~ 5–10 that would be required to make spiral galaxies dominate lens samples.

We thank A. Loeb for useful discussions, and the referee, P. Schneider, for comments on the manuscript. C. R. K. is supported by ONR-NDSEG grant N00014-93-I-0774. C. S. K is supported by NSF grant AST 94-01722 and NASA ATP grant NAG 5-4062.

REFERENCES

Alcock, C., et al. 1995, ApJ, 445, 133
Ashman, K. M. 1992, PASP, 104, 1109
Bahcall, J. N. 1984, ApJ, 276, 169
———. 1986, ARA&A, 24, 577
Bahcall, J. N., Flynn, C., & Gould, A. 1992, ApJ, 389, 234
Bartelmann, M., & Loeb, A. 1996, ApJ, 457, 529
Binney, J., & Tremaine S. 1987, Galactic Dynamics (Princeton: Princeton Univ. Press)
Buote, D. A., & Canizares, C. R. 1994, ApJ, 427, 86
———. 1996, ApJ, 457, 177
Carilli, C. L., Rupen, M. P., & Yanny, B. 1993, ApJ, 412, L59
Combes, F., & Wiklind, T. 1997, ApJ, 486, L79
de Vaucouleurs, G. 1948, Ann. d'Astrophys., 11, 247
Dubinski, J., & Carlberg, R. G. 1991, ApJ, 378, 496
Evans, N. W., & Collett, J. L. 1993, MNRAS, 264, 353
Fukugita, M., & Turner, E. L. 1991, MNRAS, 253, 99
Guthrie, B. N. G. 1992, A&AS, 93, 255
Hogg, D. W., & Blandford, R. D. 1994, MNRAS, 268, 889
Huchra, J., Gorenstein, M., Kent, S., Shapiro, I., Smith, G., Horine, E., & Perley, R. 1985, AJ, 90, 691
Jackson, N., Nair, S., & Browne, I. W. A. 1997, in Observational Cosmology with the New Radio Surveys, ed. M. Bremer, N. Jackson, & I. Perez-Fournon (Dordrecht: Kluwer), 315
Jackson, N., et al. 1995, MNRAS, 274, L25
Jaffe, W. 1983, MNRAS, 202, 995
Jauncey, D. L., et al. 1991, Nature, 352, 132
Jaunsen, A. O., & Hjorth, J. 1997, A&A, 317, 39
Kassiola, A., & Kovner, I. 1993, ApJ, 417, 459

Kauffmann, G., Charlot, S., & White, S. D. M. 1996, MNRAS, 283, L117
Keeton, C. R., & Kochanek, C. S. 1996, in Astrophysical Applications of Gravitational Lensing, ed. C. S. Kochanek & J. N. Hewitt (Dordrecht: Kluwer), 419
Keeton, C. R., Kochanek, C. S., & Falco, E. E. 1997a, preprint
Keeton, C. R., Kochanek, C. S., & Seljak, U. 1997b, ApJ, 482, 604
Kerr, F. J., & Lynden-Bell, D. 1986, MNRAS, 221, 1023
King, L. J., & Browne, I. W. A. 1996, MNRAS, 282, 67
Kochanek, C. S. 1991, ApJ, 379, 517
———. 1993, ApJ, 419, 12
———. 1996a, ApJ, 466, 638
———. 1996b, ApJ, 473, 595
Kormann, R., Schneider, P., & Bartelmann, M. 1994a, A&A, 284, 285
———. 1994b, A&A, 286, 537
Kuijken, K. 1995, in Stellar Populations, ed. P. C. van der Kruit & G. Gilmore (Dordrecht: Kluwer), 195
Kuijken, K., & Gilmore, G. 1989, MNRAS, 239, 605
———. 1991, ApJ, 367, L9
Kuzmin, G. 1956, AZh, 33, 27
Lovell, J. E. J., et al. 1996, ApJ, 472, L5
Maller, A. H., Flores, R. A., & Primack, J. R. 1997, ApJ, 486, 681
Maoz, D., & Rix, H.-W. 1993, ApJ, 416, 425
Mestel, L. 1963, MNRAS, 126, 553
Monet, D. G., Richstone, D. O., & Schechter, P. L. 1981, ApJ, 245, 454
O'Dea, C. P., Baum, S. A., Stanghellini, C., Dey, A., van Breugel, W., Deustua, S., & Smith, E. P. 1992, AJ, 104, 1320
Patnaik, A. R., Browne, I. W. A., King, L. J., Muxlow, T. W. B., Walsh, D., & Wilkinson, P. N. 1993, MNRAS, 261, 435
Persic, M., Salucci, P., & Stel, F. 1996, MNRAS, 281, 27
Rao, A. P., & Subramanyan, R. 1988, MNRAS, 231, 229
Reid, M. 1993, ARA&A, 31, 345
Rix, H.-W. 1996, in Unsolved Problems of the Milky Way, ed. L. Blitz & P. Teuben (Dordrecht: Kluwer), 23
Sackett, P. D. 1996, in Astrophysical Applications of Gravitational Lensing, ed. C. S. Kochanek & J. N. Hewitt (Dordrecht: Kluwer), 165
———. 1997, ApJ, 483, 103
Sackett, P. D., Rix, H.-W., Jarvis, B. J., & Freeman, K. C. 1994, ApJ, 436, 629
Schechter, P. L., et al. 1997, ApJ, 475, L85
Schneider, P., Ehlers, J., & Falco, E. E. 1992, Gravitational Lensing (New York: Springer)
Smette, A., Claeskens, J.-F., & Surdej, J. 1997, New Astron., 2, 53
Toomre, A. 1962, ApJ, 138, 385
Turner, E. L., Ostriker, J. P., & Gott, J. R. 1984, ApJ, 284, 1
van Albada, T. S., & Sancisi, R. 1986, Philos. Trans. R. Soc. London, A, 320, 447
van der Kruit, P. C. 1989, in The Milky Way as a Galaxy, ed. R. Buser & I. King (Geneva: Geneva Obs.), 185
Wallington, S., & Narayan, R. 1993, ApJ, 403, 517
Wang, Y., & Turner, E. L. 1997, preprint
Wiklind, T., & Combes, F. 1995, A&A, 299, 382
———. 1996, Nature, 379, 139
Wolfe, A. M. 1988, in QSO Absorption Lines: Probing the Universe, ed. J. C. Blades, D. A. Turnshek, & C. A. Norman (Cambridge: Cambridge Univ. Press), 297
———. 1995, in QSO Absorption Lines, ed. G. Meylan (Heidelberg: Springer), 13